BIOCHEMISTRY
including biophysical chemistry & molecular biology

Article

pubs.acs.org/biochemistry

Light-Mediated Hydrogen Generation in Photosystem I: Attachment of a Naphthoquinone−Molecular Wire−Pt Nanoparticle to the A_{1A} and A_{1B} Sites

Michael Gorka,[†] Jonas Schartner,[†,‡] Art van der Est,[*,§] Matthias Rögner,[‡] and John H. Golbeck[*,†,∥]

[†]Department of Chemistry, The Pennsylvania State University, University Park, Pennsylvania 16802, United States

[‡]Department of Plant Biochemistry, Faculty of Biology and Biotechnology, Ruhr-University Bochum, 44801 Bochum, Germany

[§]Department of Chemistry, Brock University, St. Catharines, ON, Canada L2S 3A1

[∥]Department of Biochemistry and Molecular Biology, The Pennsylvania State University, University Park, Pennsylvania 16802, United States

Supporting Information

ABSTRACT: The molecular wire-appended naphthoquinone 1-[15-(3-methyl-1,4-naphthoquinone-2-yl)]pentadecyl disulfide [$(NQ(CH_2)_{15}S)_2$] has been incorporated into the A_{1A} and A_{1B} sites of Photosystem I (PS I) in the *menB* variant of *Synechocystis* sp. PCC 6803. Transient electron paramagnetic resonance studies show that the naphthoquinone headgroup displaces plastoquinone-9 from the A_{1A} (and likely A_{1B}) sites to a large extent. When a Pt nanoparticle is attached to the molecular wire by reductive cleavage of the disulfide and reaction with the resulting thiol, the PS I−$NQ(CH_2)_{15}S$−Pt nanoconstruct evolves dihydrogen at a rate of 67.3 μmol of H_2 (mg of Chl)$^{-1}$ h^{-1} [3.4 e$^-$ (PS I)$^{-1}$ s^{-1}] after illumination for 1 h at pH 6.4. No dihydrogen is detected if wild-type PS I, which does not incorporate the quinone, is used or if either $(NQ(CH_2)_{15}S)_2$ or the Pt nanoparticle is absent. Time-resolved optical studies of the PS I−$NQ(CH_2)_{15}S$−Pt nanoconstruct show that the lifetimes of the forward electron transfer to and reverse electron transfer from the iron−sulfur clusters are the same as in native PS I. Thus, electrons are not shuttled directly from the quinone to the Pt nanoparticle during either forward or reverse electron transfer. It is found that the rate of dihydrogen evolution in the PS I−$NQ(CH_2)_{15}S$−Pt nanoconstruct depends strongly on the concentration the sacrificial electron donor cytochrome c_6. These observations can be explained if the iron−sulfur clusters are involved in stabilizing the electron; the ∼50 ms residence time of the electron on F_A or F_B is sufficiently long to allow cytochrome c_6 to reduce P_{700}^+, thereby eliminating the recombination channel. In the absence of P_{700}^+, slow electron transfer through the molecular wire to the Pt catalyst can occur, and hence, H_2 evolution is observed.

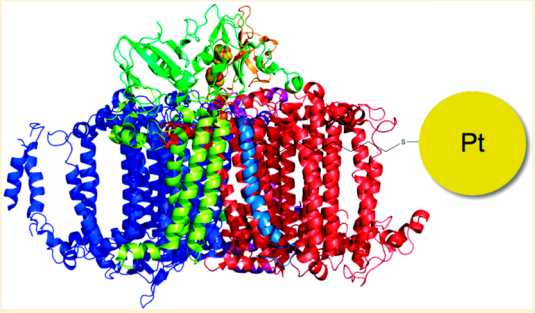

The conversion of solar radiation into stored chemical energy through entirely artificial means has proven to be challenging, often requiring low-abundance metals such as ruthenium or iridium and frequently suffering from low quantum yields. In contrast, photosynthetic reaction centers in plants and bacteria employ abundant metals such as iron, manganese, and calcium and offer impressively high quantum yields. Photosystem I (PS I), in particular, is relevant to biofuel research because it generates a low-potential reductant capable of reducing protons to dihydrogen.[1] The cofactors and the kinetics of electron transfer in PS I are depicted in Figure 1. Although the inherent lifetime of the initial charge-separated state between the donor P_{700}^+ and the acceptor A_0^- is ∼30 ns,[2] the lifetime is lengthened by electron transfer through a series of acceptors that include two phylloquinones, A_{1A} and A_{1B}, and three [4Fe-4S] clusters, F_X, F_A, and F_B. When the electron is present on any given cofactor, there is competition between forward electron transfer and backward electron transfer, the latter leading ultimately to charge recombination with P_{700}^+. Because the rates of forward electron transfer (depicted as solid lines) are typically several orders of magnitude greater than the rates of backward electron transfer (depicted as dashed lines), the quantum efficiency of electron transfer to the terminal Fe−S clusters borders on 100%.[3,4] This high quantum efficiency occurs at the expense of Gibbs free energy; nevertheless, as much as 59% of the energy of a 700 nm photon is conserved in the final $P_{700}^+F_B^-$ charge-separated state.[2]

A number of methods have been devised for attaching catalysts to PS I for light-driven dihydrogen production. In a series of pioneering applications, Greenbaum and colleagues deposited Pt, Os, or Ru onto both thylakoid membranes and PS I complexes by using the reducing power of the acceptors to generate the free metal from the salt.[5−11] These modified reaction centers evolved dihydrogen in light when supplied

Received: January 24, 2014
Revised: March 19, 2014
Published: March 20, 2014

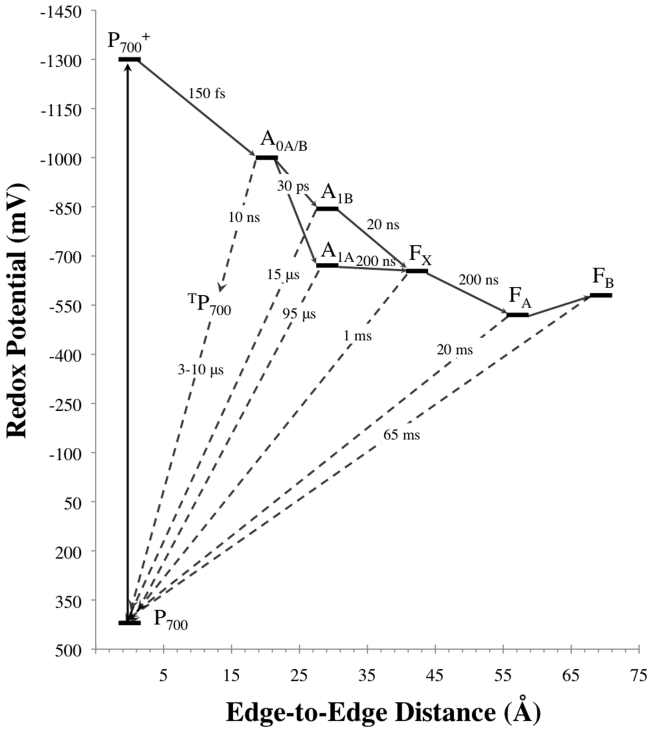

Figure 1. Depiction of the midpoint potential in millivolts (ordinate) and edge-to-edge distance (abscissa) of the PS I cofactors. The solid lines represent forward electron transfer lifetimes and dashed lines charge recombination lifetimes. Although the latter are depicted as direct to P_{700}^+, charge recombination proceeds by way of backward electron transfer to (at least) A_{1A} and A_{1B}. The A and B branches are depicted as A_{0A}/A_{1A} and A_{0B}/A_{1B}, respectively.

with sacrificial donors to P_{700}^+. The use of deposited Pt has been greatly extended by a number of other groups[12−15] in an attempt to produce a practical solar conversion device. Another method attempts to position the catalyst close to but not in intimate contact with PS I. One example is a [NiFe]-hydrogenase enzyme that has been genetically fused with PsaE and introduced into a PsaE-less variant of PS I.[16−18] The result is that the [NiFe]-hydrogenase is bound close the terminal Fe−S clusters of PS I, thereby allowing it to act as an acceptor for electrons that have been transferred from P_{700} to F_A or F_B. Another example is the use of a molecular wire to attach a Pt catalyst[19,20] or a [FeFe]-hydrogenase[23−22] to the F_B cluster of PS I. The molecular wire similarly restricts the range of distances between the electron transfer cofactors, making it suitable for rapid electron transfer. Both methods allow the electron to tunnel from the terminal iron−sulfur cluster to the catalyst in a short period of time,[24] and both report high rates of generation of dihydrogen under illumination.

The question of whether it is possible to extract the electron from an earlier acceptor in PS I arises. Steric constraints imposed by the PsaA−PsaB heterodimer make it difficult to devise a method for attaching a molecular wire to the F_X cluster. However, a variety of techniques exist to introduce alternative quinones into the A_{1A} and A_{1B} sites. Solvent extraction with diethyl ether[25−30] or a hexane/methanol mixture[32,31] removes the majority of the chlorophylls and most, if not all, of the quinones and carotenoids, allowing a wide range of naphthoquinones,[26,28,30,31,33] anthraquinones,[34,35] and some benzoquinones[36−38] to be incorporated into the A_{1A} and A_{1B} sites. This method was recently exploited by Terasaki et al.,[39] who introduced the substituted naphthoquinone, $NQ(CH_2)_{15}S$-Au, into the A_{1A} and A_{1B} sites to fabricate a biophotosensor. A genetic method for introducing alternative quinones is also available, which involves interruption of the *menA*, *menB*, *menD*, or *menE* gene.[40−44] With any of these genes inactivated, the biosynthesis of phylloquinone is blocked, and plastoquinone-9 acts as a surrogate in the A_{1A} and A_{1B} sites. Plastoquinone-9 is loosely bound and can be displaced with a variety of substituted naphthoquinones[43,45,46] or anthraquinones.[47] This method of quinone exchange has an advantage over solvent extraction in that all of the chlorophylls and carotenoids are retained in the PS I complexes.

For electrons to be transferred from the terminal iron−sulfur clusters through an alternative pathway, one of two conditions must be met. Either the rate of forward electron transfer through the alternative pathway must exceed the rate of the back reaction to P_{700}^+, or the rate of reduction of P_{700}^+ by an external donor must exceed the rate of the back reaction so that recombination is prevented. Because of the long lifetime (65 ms) of the $P_{700}^+[F_A/F_B]^-$ charge-separated state, either of these conditions is readily met when a molecular wire incorporating a Pt nanoparticle or a [FeFe]-hydrogenase enzyme is attached to the terminal F_B cluster. However, a more complicated situation is encountered if the electron is to be removed from A_{1A} and A_{1B}. Because the quinone is not the terminal acceptor, the electrons must be transferred to the catalyst during either the forward reaction or the back reaction. For the forward reaction, the rate of electron transfer along the alternative pathway must exceed that of electron transfer from the quinone to F_X. However, if the electron is transferred during the back reaction, then reduction of P_{700}^+ must outcompete the recombination.

In this study, we extend the work of Teraskai et al.[39] to determine whether a construct based on Pt instead of Au can generate dihydrogen under illumination and whether the transfer of the electrons from the A_{1A} and A_{1B} sites occurs during the forward reaction or the back reaction. We expect that the Pt nanoparticle will not be able to penetrate into the hydrophobic region of the protein; thus, the alkyl chain must be long enough to span the distance between the A_1 site(s) and the surface of the protein. On the other hand, the rate of electron transfer between the quinone and the nanoparticle is expected to decrease as the length of the tether increases. Thus, there should be an optimal length for the tether corresponding to the minimal distance between the A_1 site and the protein surface. On the basis of the structure, we estimate this distance to be on the order of half the transmembrane distance of 30 Å. The length of the alkyl tether depends on its conformation, but the maximal length of a 15-carbon alkyl chain is roughly 22.5 Å. Hence, a construct with a 15-carbon chain should be sufficient to span the distance. This substituted naphthoquinone can be incorporated into the A_{1A} and A_{1B} sites of *menB* PS I complexes by displacing the exchangeable plastoquinone-9. We show that when the naphthoquinone is tethered to a Pt nanoparticle, it can still be exchanged into the A_{1A} and A_{1B} binding sites and that this construct generates dihydrogen upon illumination. However, we also show that the rate of dihydrogen production depends on the concentration of the external donor, cytochrome c_6 (Cyt c_6), present in solution. Thus, we propose that the trapping occurs during the back reaction and that the iron−sulfur clusters are involved in stabilizing the electron, thereby allowing a longer residence time that permits cytochrome c_6 to reduce P_{700}^+ and eliminate the recombination channel.

dx.doi.org/10.1021/bi500104r | *Biochemistry* 2014, 53, 2295−2306

MATERIALS AND METHODS

Synthesis of 1-[15-(3-Methyl-1,4-naphthoquinone-2-yl)]pentadecyl Disulfide. 1-[15-(3-Methyl-1,4-naphthoquinone-2-yl)]pentadecyl disulfide [$(NQ(CH_2)_{15}S)_2$] was synthesized in accordance with the literature[39] and purified via a modified procedure. The method is shown in Scheme 1.

Scheme 1. Synthesis of 1-[15-(3-Methyl-1,4-naphthoquinone-2-yl)]pentadecyl Disulfide

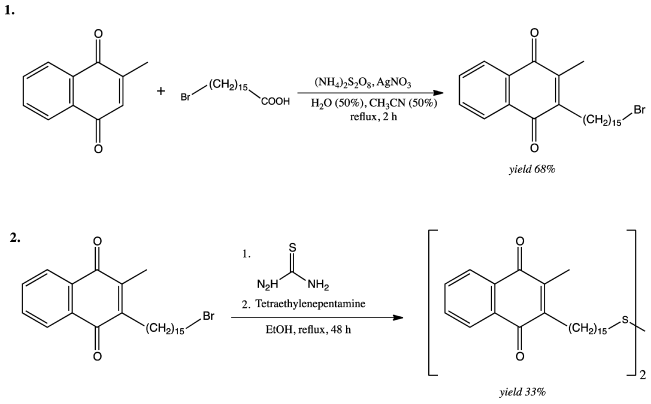

Menadione was reacted for 2 h with ω-bromohexadecanoic acid in the presence of silver nitrate and ammonium persulfate. The bromide was then converted into the corresponding thiol group by refluxing with thiourea and via exclusion of dioxygen for 24 h, followed by the addition of tetraethylenepentamine and refluxing for an additional 24 h. The product was characterized by 400 MHz ^{1}H nuclear magnetic resonance, Fourier transform infrared spectroscopy, and mass spectrometry. The full procedure and characterization data are provided in the Supporting Information.

Preparation of Pt Nanoparticles. Pt nanoparticles were prepared according to literature procedures.[48] One milliliter of mercaptosuccinic acid (23.7 mM) and 10 mL of hexachloroplatinic acid (3.38 mM) were mixed and stirred vigorously in 18.2 MΩ H_2O. Five milliliters of sodium borohydride (67.6 mM) was added to the reaction solution. The mixture immediately turned from yellow to brown. The reaction was completed when the solution turned dark brown. The resulting particles were characterized via transmission electron microscopy and determined to be 3−5 nm in diameter.

Photosystem I Growth and Purification. Wild-type PS I complexes were isolated from *Synechocystis* sp. PCC 6803 and purified in accordance with the literature.[49] The purified PS I trimers were resuspended in buffer containing 0.05% (v/v) Triton X-100 and 20% (v/v) glycerol in 50 mM Tris-HCl (pH 8.3). The *menB* variant was grown and purified according to published methods.[40] Cells were grown in β-HEPES medium supplemented with 5 mM glucose and 25 μg/mL spectinomycin. PS I trimers from the variant were isolated using the same protocol that was used for the wild type with the exception that β-dodecyl maltoside (β-DM) was used instead of Triton X-100.

Incorporation of Quinone into the *menB* Variant of PS I. Quinone incorporation for transient electron paramagnetic resonance (EPR) and time-resolved optical studies was achieved via a 16−24 h incubation of *menB* PS I with a 100-fold excess of either phylloquinone or $(NQ(CH_2)_{15}S)_2$. The sample was washed twice with Tris-HCl (pH 8.3) containing 0.05% β-DM over a 50 kDa Centricon membrane to remove both the residual naphthoquinone and the displaced plastoquinone.

Nanoconstruct Assembly and Dihydrogen Analysis. The $NQ(CH_2)_{15}S$−Pt adduct was made by reductive cleavage of $(NQ(CH_2)_{15}S)_2$ by the Pt nanoparticles *in situ*. The concentration of Pt in the nanoparticle reaction mixture was 2.11 mM. On the basis of the atomic radius of Pt and the nanoparticle radius of ∼4 nm and assuming close packing of the atoms, there should be $\sim 10^4$ atoms per nanoparticle. Hence, the concentration of Pt nanoparticles in the reaction mixture was ∼0.2 μM. A total of 2 mL of the Pt nanoparticles was incubated with 100 μL of a 20 mM solution of the target naphthoquinone in the dark while the mixture was vigorously stirred for >7 days. The nanoconstruct was assembled via a 16−24 h incubation of 75 μL of the $NQ(CH_2)_{15}S$−Pt adduct, *menB* or wild-type (WT) PS I at a final concentration of 5.8 μg/mL chlorophyll (6.5 μM P_{700}), and either Tris or MES buffer at pH 8.3 or 6.4, respectively, to a final volume of 250 μL. Following incubation, soluble electron donors were added to final concentrations of 30 μM DPIP, 100 mM ascorbate, and 100 μM cytochrome c_6. For experiments monitoring the effect of cytochrome concentration, the PSI concentration was increased to 50 μg/mL, and the donor concentrations were changed to 10 μM DPIP, 5 mM sodium ascorbate, and 0−100 μM cytochrome c_6. The headspaces of the assembled nanoconstruct solutions were purged in the dark for 10 min using ultrapure argon and samples were exposed to continuous illumination using a 100 W xenon arc lamp (996 μmol of photons m^{-2} s^{-1}). The temperature was maintained using a clear polycarbonate flask filled with ddH_2O to remove infrared radiation. Periodically, 200 μL of headspace was removed with an airtight locking syringe and analyzed with a Shimadzu GC-8A gas chromatograph equipped with a ShinCarbon 80/100 column (2 m × 2 mm) and thermal conductivity detector (detector current of 100 mA) with ultrapure N_2 as the carrier gas (flow rate of 0.75 mL/min).

Transient EPR Spectroscopy. Time/field transient EPR data sets were measured using a modified ER 200D-SRC spectrometer with either a Bruker ER 041 X-MR X-band or a Bruker ER 051 QR Q-band microwave bridge. For the X-band measurements, a Flexline ER 4118 X-MD-5W1 dielectric resonator was used, and for the Q-band experiments, an ER 5106 QT-W cylindrical resonator was used. A Surelight-Continuum Nd:YAG laser operating at 10 Hz and a wavelength of 532 nm and 4.0 mJ/pulse provided single-turnover flashes. The temperature was controlled using an Oxford Instruments CF935 gas flow cryostat. The transient EPR signal was collected in direct detection mode with a home-built broadband amplifier (bandwidth of >500 MHz), digitized using a LeCroy LT322 500 MHz digital oscilloscope, and saved on a personal computer for analysis. Samples were pretreated with 1 mM sodium ascorbate and 50 μM phenazine methosulfate (PMS) prior to analysis. The samples were adapted to the dark for 20 min on ice to ensure complete reduction of P_{700}^+ and frozen in the dark before being illuminated.

Time-Resolved Optical Studies at 820 and 480 nm. Forward and reverse electron transfer kinetics in the PS I samples was monitored by transient absorbance changes at 480 and 820 nm following a single-turnover laser flash at 532 nm using a laboratory-built, dual-beam spectrometer as described previously.[50] Samples were placed in a 10 mm × 2 mm quartz cuvette. The cuvette was placed such that the optical path length was 10 mm. The measuring and reference beam

dx.doi.org/10.1021/bi500104r | *Biochemistry* 2014, 53, 2295−2306

intensities were balanced using a variable density optical filter wheel. The difference signal was amplified with a model 11A33 differential comparator and processed using a DSA610 digital signal analyzer (Tektronix, Beaverton, OR). Measurements at 480 nm included a 480 laser diode (OptoEngine MBL-H-480-30mW) as the measuring beam and a mechanical shutter that opened the measuring beam 2 ms prior to the flash. The spectrometers were controlled using software written in LabView (National Instruments), and the data were analyzed using the graphics capability of IGOR (Wavemetrics). The samples contained 50 μg/mL chlorophyll, Tris-HCl (pH 8.3), 10 μM DPIP, 5 mM sodium ascorbate, and 0.05% (w/v) β-DM.

RESULTS

Transient EPR Spectroscopy. Our first objective was to confirm that plastoquinone-9 could be displaced by $(NQ(CH_2)_{15}S)_2$ in *menB* PS I. We used $(NQ(CH_2)_{15}S)_2$ rather than $NQ(CH_2)_{15}SH$ in the incorporation studies with the *menB* variant to prevent reactions with the reactive sulfhydryl group. At low temperature, reversible electron transfer in PS I occurs repeatedly between P_{700} and A_{1A}, resulting in the spin-polarized $P_{700}^{\bullet+}A_{1A}^{\bullet-}$ radical pair that can be observed by transient EPR (TREPR) (see ref 51 for a short overview). The TREPR spectrum is sensitive to the structure and orientation of the quinone as well as its interaction with its binding site. Low-temperature TREPR spectra of wild-type PS I and *menB* PS I before and after incubation with $(NQ(CH_2)_{15}S)_2$ are shown at X-band (Figure 2A) and Q-band (Figure 2B). The spectra of the wild-type and *menB* samples are similar to those reported previously,[42] and at both microwave frequencies, changes after incubation with $(NQ(CH_2)_{15}S)_2$ are seen primarily in the low-field region of the spectrum, which is dominated by contributions from $A_{1A}^{\bullet-}$, while the high field region, where the contributions from $P_{700}^{\bullet+}$ appear, is largely unchanged. At Q-band, the components of the quinone **g** tensor are partially resolved and the spectra are sensitive to *g* anisotropy. The delocalization of the electron over two rings in the naphthoquinone headgroups of $(NQ(CH_2)_{15}S)_2$ and phylloquinone leads to a *g* anisotropy smaller than that of plastoquinone-9, which contains a benzoquinone headgroup with only one ring. The difference between the structure of the two quinones results in an upfield shift of the features in the quinone portion of the Q-band spectrum after incubation (Figure 2B).

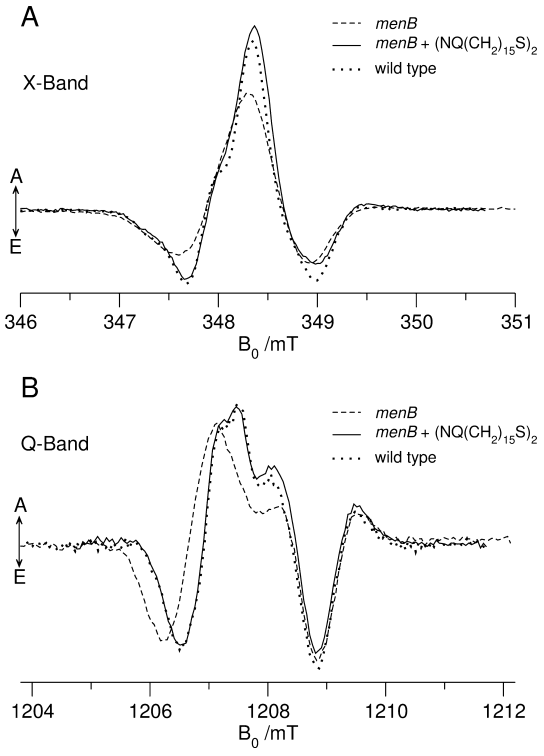

Figure 2. TREPR spectra of PS I at 90 K. Comparison of WT PS I with *menB* PS I before and after incubation with $(NQ(CH_2)_{15}S)_2$ at (A) X-band and (B) Q-band. *A* equals absorption, and *E* equals emission.

The Q-band spectrum of the PS I–$(NQ(CH_2)_{15}S)_2$ sample (Figure 2B, solid spectrum) is almost identical to that of wild-type PS I (Figure 2B, dotted spectrum), which is expected, as phylloquinone and $(NQ(CH_2)_{15}S)_2$ have the same headgroup. At X-band, the *g* anisotropy is not resolved and the spectrum is more sensitive to hyperfine couplings than at Q-band. In plastoquinone-9, the two methyl groups and the methylene group of the side chain have significant hyperfine couplings, which overlap to give a broad inhomogeneous line shape.[42] In the wild-type and $(NQ(CH_2)_{15}S)_2$ samples, the presence of only a single methyl group leads to a decrease in the inhomogeneous line width, and as a result, the height of the central absorption and low-field emission increases. In WT PS I, the fact that the C_4 carbonyl group is H-bonded to the protein while the C_1 carbonyl group is not results in high electron density on C_2 of the naphthoquinone ring[52] and leads to prominent, albeit only partially resolved, hyperfine splitting from the 2-methyl group.[53] This splitting is most evident as a shoulder on the low-field side of the central absorptive peak (Figure 2A). Although the X-band spectrum of the PS I–$(NQ(CH_2)_{15}S)_2$ sample (Figure 2A, solid spectrum) is almost identical to that of WT PS I (Figure 2A, dotted spectrum), the shoulder due to the 2-methyl hyperfine splitting is slightly less pronounced.

There are several possible reasons for this difference. One is that the long side chains in phylloquinone and $(NQ(CH_2)_{15}S)_2$ may have different orientations of the first methylene group relative to the quinone ring. The hyperfine couplings of the two methylene protons depend on this orientation, and an increase in their values would increase the inhomogeneous line width and lower the resolution of the 2-methyl hyperfine splitting. Another is that the spin density distribution on the naphthoquinone headgroup may differ slightly in the two quinones such that the density on C_2 is lower in the $(NQ(CH_2)_{15}S)_2$ sample. It is also possible that the sample incubated with $(NQ(CH_2)_{15}S)_2$ still contains a small amount of residual plastoquinone-9 in the A_{1A} site, which would also tend to lower the resolution of the spectrum. Even though TREPR does not directly provide information about the A_{1B} site, it can be assumed on the basis of the structural similarity with the A_{1A} site that $(NQ(CH_2)_{15}S)_2$ has similarly displaced plastoquinone-9.

The TREPR data show that $(NQ(CH_2)_{15}S)_2$ has a high affinity for the A_{1A} (and presumably A_{1B}) binding site without the Pt nanoparticle attached. Corresponding experiments with the Pt nanparticle bound to the tether are not feasible because the nanoparticles aggregate and precipitate at the concentrations needed for EPR experiments. However, time-resolved

dx.doi.org/10.1021/bi500104r | *Biochemistry* 2014, 53, 2295–2306

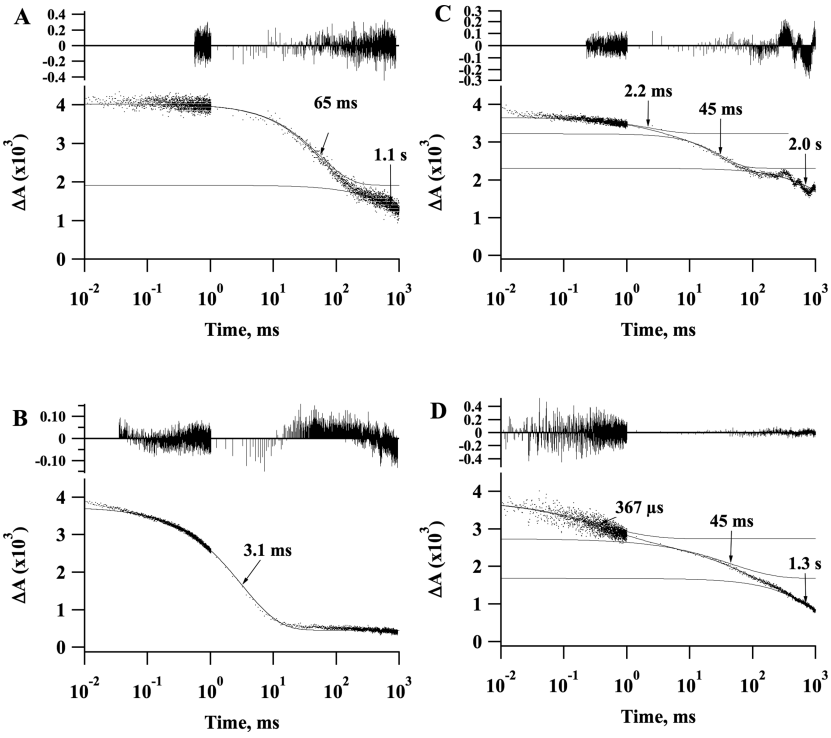

Figure 3. Time-resolved optical spectra measured at 820 nm after a saturating laser flash: (A) WT PS I, (B) *menB* PS I, (C) *menB* PS I incubated with $(NQ(CH_2)_{15}S)_2$, and (D) *menB* PS I incubated with the $NQ(CH_2)_{15}S$−Pt adduct. The data are shown as dots, and the fitted spectra are shown as solid lines. The residual of the fit is depicted above each of the plots. The long-lived phase in the spectra represents the transfer of an electron from the external donor in reaction centers that have lost the electron on the acceptor side to dioxygen. The reaction mixture contained PS I at 50 μg/mL Chl, 5 mM sodium ascorbate, 10 μM DPIP, and 0.05% β-DM in 50 mM Tris buffer (pH 8.3).

optical spectroscopy, which can be performed at lower concentrations, can be used to characterize the incorporation.

Time-Resolved Optical Spectroscopy at 820 nm. Flash excitation of PS I leads to an absorbance change at 820 nm due to the formation P_{700}^+, and the kinetics of this absorbance change can be used to monitor the back reaction from the acceptor side of the complex. The following experiments were conducted in the absence of cytochrome c_6 so that the back reaction kinetics would not be obscured by rapid forward donation to P_{700}^+. In WT PS I, two major kinetic components are observed after a laser flash (Figure 3A). The event with a lifetime of 65 ms represents $P_{700}^+[F_A/F_B]^-$ recombination, and the component with a lifetime of 1.1 s represents donation of an electron from DPIP to P_{700}^+ in those reaction centers in which the electron has been lost to dioxygen. In *menB* PS I, which contains plastoquinone-9 in the A_{1A} and A_{1B} binding sites, the amplitude of the absorbance change [3.7 milli-optical density units (mOD)] is slightly lower than that of the WT (4 mOD) and $P_{700}^+[F_A/F_B]^-$ recombination is accelerated, showing a lifetime of 3.1 ms (Figure 3B). A minor component with a (long) lifetime unresolved on this time scale is also present, which represents donation of an electron from DPIP to P_{700}^+. The faster recombination between P_{700}^+ and $[F_A/F_B]^-$ in *menB* PS I occurs because the midpoint potential of plastoquinone-9 is more oxidizing than that of phylloquinone. This results in a smaller Gibbs free energy difference between A_{1A} or A_{1B} and F_X, thereby increasing the population of electrons on the quinone relative to the FeS clusters. Because charge recombination proceeds by backward transfer of an electron from $[F_A/F_B]^-$ through F_X and A_{1A}/A_{1B}, the change in relative populations leads to faster depletion of the electrons from the Fe−S clusters and, hence, faster reduction of P_{700}^+.[54] The smaller amplitude of the slow kinetic phase is due to the residence time of the electron on F_B being shorter in *menB* PS I. The probability of an electron being transferred from F_B^- to dioxygen is correspondingly lower.

When $(NQ(CH_2)_{15}S)_2$ is added to *menB* PS I (Figure 3C), the amplitude of the absorbance change at the onset of the flash (3.6 mOD) is similar to that of the *menB* variant (3.7 mOD), but the 3.1 ms kinetic phase is largely replaced by two kinetic phases with lifetimes of 45 ms (0.9 mOD) and 2.0 s (2.3 mOD). The 2.2 ms kinetic phase (0.4 mOD) is similar to that of the dominant kinetic phase in the *menB* variant and is assigned to a minor fraction of PS I complexes that still contain plastoquinone-9. The 45 ms and 2.0 s events are similar to those seen in WT PS I (Figure 3A) and are due to $P_{700}^+[F_A/F_B]^-$ recombination and donation of an electron from DPIP to P_{700}^+, respectively. The resumption of a long-lived charge-separated state is consistent with replacement of plastoquinone-9 with a naphthoquinone, and with forward electron donation to F_A and F_B. When the $NQ(CH_2)_{15}S$−Pt adduct was incubated with *menB* PS I (Figure 3D), the total amplitude of the absorbance change at the flash was similar to that of the *menB* variant. However, the 45 ms and 1.3 s kinetic events are present as in the WT, indicating that the majority of the electrons are similarly transferred to the iron−sulfur clusters. This result shows that the $NQ(CH_2)_{15}S$−Pt adduct is able to displace plastoquinone in the *menB* variant but also implies that the transfer of an electron to the Pt nanoparticle does not compete with forward transfer to the iron−sulfur clusters. The origin of the minor, 370 μs event is unknown; however, it does represent a return of an electron to P_{700}^+. Because of the distance involved, we consider it unlikely that this event represents

dx.doi.org/10.1021/bi500104r | *Biochemistry* 2014, 53, 2295−2306

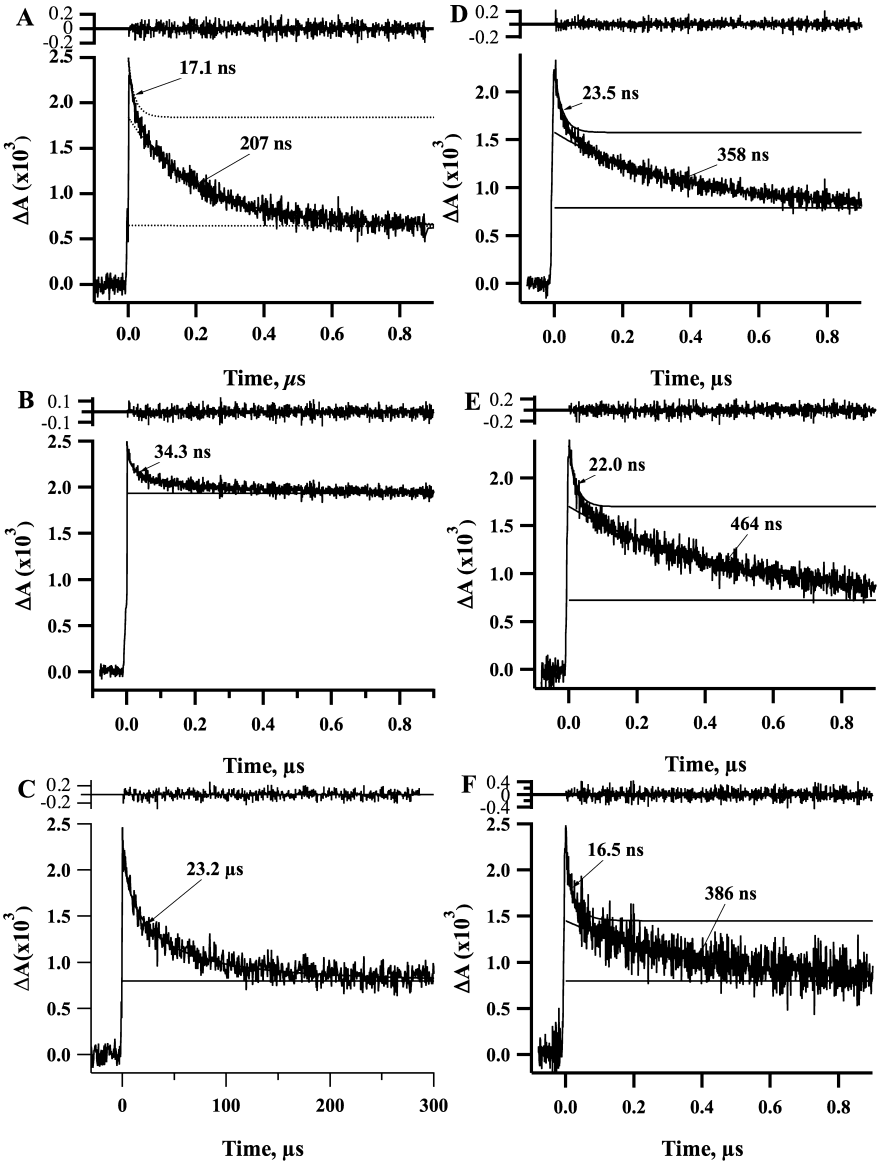

Figure 4. Time-resolved optical spectra measured at 480 nm after a saturating laser flash: (A) WT PS I, (B) *menB* PS I, (C) *menB* PS I on a microsecond time scale, (D) *menB* PS I incubated with phylloquinone, (E) *menB* PS I incubated with $(NQ(CH_2)_{15}S)_2$, and (F) *menB* PS I incubated with the $NQ(CH_2)_{15}S$–Pt adduct. The data are shown as dots, and the fitted spectra are shown as solid lines. The residual of the fit is depicted above each of the plots. Because P_{700} also absorbs at this wavelength, the long-lived phase in the spectra represents long-lived P_{700}^+ that does not decay on this time scale. The reaction mixture contained PS I at 50 μg/mL Chl, 5 mM sodium ascorbate, 10 μM DPIP, and 0.05% β-DM in 50 mM Tris (pH 8.3).

recombination between an electron on the Pt nanoparticle and P_{700}^+.

Time-Resolved Optical Spectroscopy at 480 nm. Electron transfer beyond A_{1A} and A_{1B} can be studied more directly using time-resolved optical absorption spectroscopy at 480 nm, a wavelength that detects the electrochromic band shift of carotenoids in the vicinity of the quinones.[55,56] The measurement at 480 nm is a proxy for the transient redox changes of the quinones and is more reliable than the measurement at 380 nm because the amplitude of the absorbance change does not depend on the identity of the quinone occupying the A_{1A} and A_{1B} sites. In WT PS I, two kinetic components are observed after a laser flash (Figure 4A). The event with a lifetime of 17.1 ns represents the forward transfer of an electron from A_{1B}^- to F_X, and the event with a lifetime of 207 ns represents the transfer of an electron from A_{1A}^- to F_X.[57] The fast and slow components are present in a ratio of 30:70, which is typical for cyanobacterial PS I. In *menB* PS I, two kinetic events are resolved, a minor component with a lifetime of 34.3 ns (Figure 4B) and a major component with a lifetime of 23.2 μs (Figure 4C; note the different time scale). The fast and slow components are present in a ratio of 25:75. The slow phase is consistent with a previous study in which a major kinetic phase with a lifetime of ∼15 μs was assigned to the transfer of an electron from plastoquinone to F_X in *menB* PS I.[41] The origin of the 34 ns phase is uncertain. At least two kinetic phases of forward electron transfer to F_X are expected when plastoquinone-9 occupies the A_{1B} and A_{1A} sites, and as discussed in ref 41, it is possible that a broad distribution of kinetic phases exists. (Further characterization of these kinetic components is beyond the scope of this work.) When native phylloquinone is incubated with *menB* PS I, two components,

dx.doi.org/10.1021/bi500104r | *Biochemistry* 2014, 53, 2295−2306

with lifetimes of 23.5 and 358 ns, are resolved that are similar to the lifetimes of the transfer of an electron from A_{1B}^- and A_{1A}^- to F_X in WT PS I (Figure 4D). This result shows that phylloquinone largely displaces plastoquinone-9 in *menB* PS I.[43] Similarly, when $(NQ(CH_2)_{15}S)_2$ is incubated with *menB* PS I, two components, with lifetimes of 22.0 and 454 ns, are resolved (Figure 4E) that resemble the fast and slow kinetic phases, respectively, in phylloquinone-reconstituted *menB* PS I. When the $NQ(CH_2)_{15}S$–Pt nanoparticle adduct is incubated with *menB* PS I (Figure 4F), two components, with lifetimes of 16.5 and 386 ns, are similarly resolved that resemble the fast and slow kinetic phases, respectively, in phylloquinone-reconstituted *menB* PS I. (The lower signal-to-noise ratio in this sample is due to a greater amount of scattering of the measuring beam in the sample containing a Pt nanoparticle.) This result is consistent with the study conducted at 820 nm, and together, the data indicate that the majority of electrons are transferred to the F_X cluster and further to F_A and F_B. It also confirms that (i) the presence of the Pt nanoparticle does not interfere with the ability of the naphthoquinone group to occupy the A_{1A} and A_{1B} sites and (ii) the similar amplitudes illustrate a nearly quantitative displacement of plastoquinone-9.

Light-Induced Dihydrogen Generation. We next tested whether the PS I–$NQ(CH_2)_{15}S$–Pt construct could evolve dihydrogen in the light. These experiments were conducted at a low chlorophyll concentration, 5.8 μg/mL, to minimize self-shielding. A detailed time course for dihydrogen production under constant illumination at pH 6.4 in the presence of 100 μM cytochrome c_6 is shown in Figure 5. After a rapid rise, the rate of dihydrogen evolution reached a maximum of 42.5 μmol of H_2 (mg of Chl)$^{-1}$ h^{-1} [2.2 e$^-$ (PS I)$^{-1}$ s^{-1}] after illumination for 1 h; thereafter, the rate declined with a half-time of ~9 h. In a series of triplicate runs, the maximal rate of dihydrogen production was 67.6 ± 8.2 μmol of H_2 (mg of Chl)$^{-1}$ h^{-1} [3.4 e$^-$ (PS I)$^{-1}$ s^{-1}] at pH 6.4 and 44.3 μmol of H_2 (mg of Chl)$^{-1}$ h^{-1} [2.3 e$^-$ (PS I)$^{-1}$ s^{-1}] at pH 8.3, both measured after illumination for 1 h (Table 1).

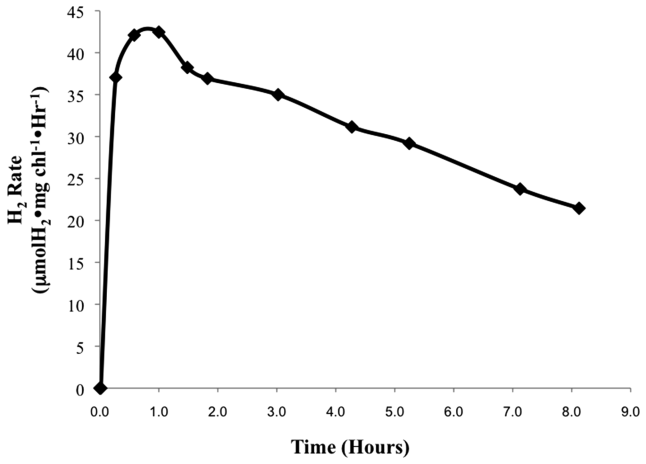

Figure 5. Time course of the rate of dihydrogen evolution during illumination of the PS I–$NQ(CH_2)_{15}S$–Pt construct at pH 6.4. The reaction mixture contained wild-type PS I at 5.8 μg/mL Chl, 100 mM sodium ascorbate, and 30 μM DPIP in 20 mM MES buffer (pH 6.5).

The controls for these experiments are listed in Table 1. No dihydrogen was detected (i) in the presence of WT PS I, the $NQ(CH_2)_{15}S$–Pt construct, Cyt c_6, and light; (ii) in the presence of *menB* PS I, Pt nanoparticles, Cyt c_6, and light but in the absence of $(NQ(CH_2)_{15}S)_2$; (iii) in the presence of *menB* PS I, Cyt c_6, and light but in the absence of the $NQ(CH_2)_{15}S$–Pt construct; (iv) in the presence of *menB* PS I, $(NQ(CH_2)_{15}S)_2$, Cyt c_6, and light but in the absence of Pt nanoparticles; (v) in the presence of *menB* PS I, the $NQ(CH_2)_{15}S$–Pt construct, and light but in the absence of Cyt c_6; or (vi) in the presence of *menB* PS I, the $NQ(CH_2)_{15}S$–Pt construct, and Cyt c_6 but in the absence of light. The detection limit for dihydrogen after illumination for 1 h was 0.034 μmol of H_2 (mg of Chl)$^{-1}$ h^{-1}.

Table 1

sample	rate of H_2 production [μmol of H_2 (mg of Chl)$^{-1}$ h^{-1}]
menB PS I, $NQ(CH_2)_{15}S$–Pt, Cyt c_6, pH 6.5, *hv*	67.3 ± 8.2[a]
menB PS I, $NQ(CH_2)_{15}S$–Pt, Cyt c_6, pH 8.3, *hv*	44.3 ± 5.3[a]
WT PS I, $NQ(CH_2)_{15}S$–Pt, Cyt c_6, pH 6.5, *hv*	0.0[a,b]
menB PS I, Pt, Cyt c_6, pH 6.5, *hv*	0.0[a,b]
menB PS I, Cyt c_6, pH 6.5, *hv*	0.0[a,b]
menB PS I, $(NQ(CH_2)_{15}S_2)$, Cyt c_6, pH 6.5, *hv*	0.0[a,b]
menB PS I, $NQ(CH_2)_{15}S$–Pt, pH 6.5, *hv*	0.0[a,b]
menB PS I, $NQ(CH_2)_{15}S$–Pt, Cyt c_6, pH 6.5	0.0[a,b]

[a]After illumination for 1 h. [b]Detection limit of 0.034 μmol of H_2 (mg of Chl)$^{-1}$ h^{-1}.

Effect of Cytochrome c_6 on Rates of Dihydrogen Production and P_{700}^+ Reduction. The question is how dihydrogen can be evolved if there is no evidence of altered electron transfer through the acceptor chain. If, as the transient absorbance data indicate, the electrons are transferred to the FeS clusters rather than through the molecular wire to the Pt nanoparticle, we would expect that dihydrogen would be evolved only at electron donor concentrations that suppress the recombination between P_{700}^+ and $[F_A/F_B]^-$. Under these conditions, the electron would equilibrate among the acceptors, but the slow kinetic leak through the span of the molecular wire would ultimately lead to trapping of the electron on the Pt nanoparticle. We therefore studied the effect of cytochrome c_6 concentration on the rate of dihydrogen produced in the PS I–$NQ(CH_2)_{15}S$–Pt construct. To correlate the results with the 820 and 480 nm optical studies shown in Figures 3 and 4, the experiment was conducted at a Chl concentration 10-fold higher than those of the experiments reported in Table 1. This results in significant self-shading, which leads to a lower rate of evolution of dihydrogen on a per Chl basis. As shown in Figure 6, no dihydrogen was detected if only the sacrificial donor, ascorbic acid, or if only ascorbic acid and 30 μM DCPIP are used as donors. Similarly, no dihydrogen was detected in the additional presence of either 0.01 or 0.1 μM cytochrome c_6. When the concentration of cytochrome c_6 was increased to 2 μM, however, dihydrogen was detected [0.05 μmol of H_2 (mg of Chl)$^{-1}$ h^{-1}], and doubling the concentration of cytochrome c_6 to 4 μM resulted in a 10-fold increase in the rate of dihydrogen evolved [1.05 μmol of H_2 (mg of Chl)$^{-1}$ h^{-1}]. Increasing the concentration of cytochrome c_6 to 100 μM resulted in a doubling of the rate of dihydrogen evolved [2.65 μmol of H_2 (mg of Chl)$^{-1}$ h^{-1}], but higher concentrations of cytochrome c_6 led to only marginally higher rates. The absence of a linear relationship between cytochrome c_6 concentration

dx.doi.org/10.1021/bi500104r | *Biochemistry* 2014, 53, 2295–2306

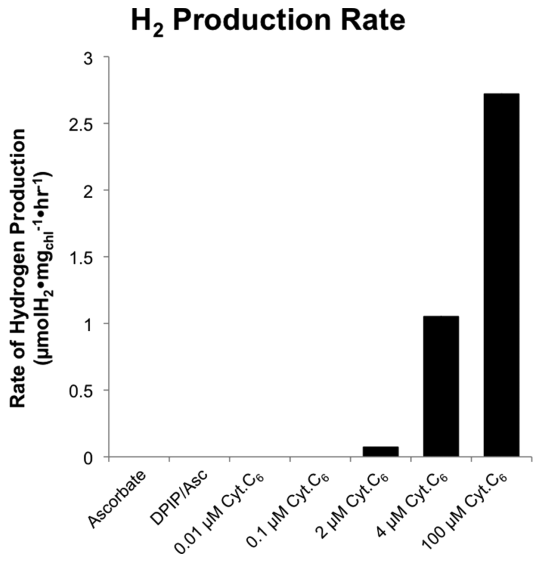

Figure 6. Bar graph depicting the rate of dihydrogen evolution as a function of external electron donors. The reaction mixture contained WT PS I at 50 μg/mL Chl in 50 mM Tris buffer (pH 8.3). Ascorbic acid and DPIP were present at concentrations of 5 mM and 10 μM, respectively, in all but the ascorbate-only experiment.

and dihydrogen production and the abrupt onset of light-induced dihydrogen production at 2 μM cytochrome c_6 indicate that more than simple kinetics is governing the reaction.

Figure 7 plots the rate of reduction of P_{700}^+ as a function of cytochrome c_6 concentration. Note that the abscissa is plotted on a logarithmic scale. In the presence of only ascorbic acid, or in the additional presence of 30 μM DPIP, the e^{-1} lifetime of P_{700}^+ is ~65 ms (compare to Figure 3A); hence, P_{700}^+ reduction is dominated by recombination from $[F_A/F_B]^-$. Under these conditions, the forward transfer of an electron to P_{700}^+ is so slow that it cannot outcompete charge recombination. When cytochrome c_6 is added to the reaction mixture, the forward transfer of an electron to P_{700}^+ is similarly outcompeted by charge recombination at concentrations of 100 nM and 0.1 μM. However, at cytochrome c_6 concentrations of >1 μM, the forward transfer of an electron to P_{700}^+ is faster than recombination according to the following sequence (values of $t_{1/2}$ in parentheses): 1 μM (45 ms), 4 μM (28 ms), 16 μM (12 ms), 50 μM (3 ms), and 100 μM (1.2 ms). From Figure 6, it is clear that dihydrogen is evolved only at cytochrome c_6 concentrations of >1 μM. Hence, dihydrogen evolution occurs only under conditions where the recombination channel from $[F_A/F_B]^-$ to P_{700}^+ is eliminated. We suggest that the iron–sulfur clusters are involved in stabilizing the electron in the PS I–NQ$(CH_2)_{15}$S–Pt construct because the longer residence time they afford allows the recombination channel to be eliminated by the forward donation of an electron to P_{700}^+.

DISCUSSION

A useful way to describe electron transfer in PS I is by the spreading of equilibrium model,[54,58] which takes as its foundation the experimental finding that the closer the reaction is to the primary charge separation step, the larger the rate constant (Figure 1). The spreading of equilibrium model takes into account the observation that at each step, the forward rate constant is considerably larger than the backward charge recombination rate constant, usually by several orders of magnitude. Accordingly, the process of light-driven electron transfer can be considered a series of steps in which all of the previous steps are in quasi-equilibrium. The equilibrium process spreads sequentially over time from the picosecond domain to

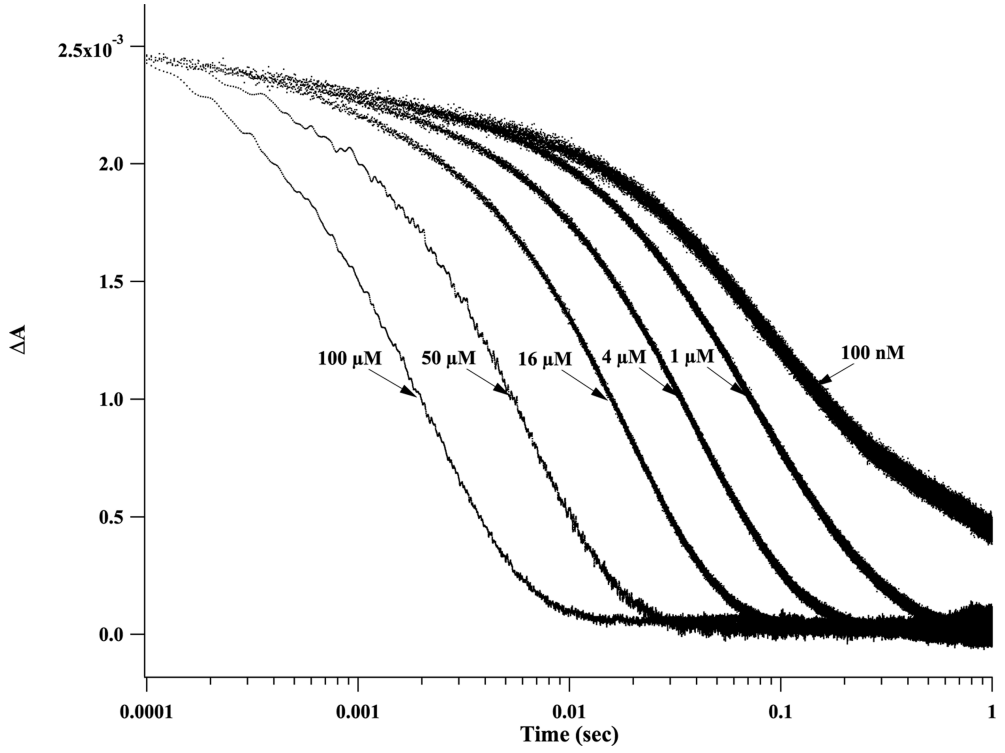

Figure 7. Time course of P_{700}^+ reduction as a function of cytochrome c_6 concentration. The reaction mixture contained WT PS I at 50 μg/mL Chl, 5 mM sodium ascorbate, and 10 μM DPIP in 50 mM Tris buffer (pH 8.3).

dx.doi.org/10.1021/bi500104r | Biochemistry 2014, 53, 2295–2306

the millisecond domain, terminating in a final quasi-equilibrium state. When this state is achieved, the electron has a finite probability of residing on each of the electron acceptors, the amount depending on the equilibrium constant separating any given acceptor−donor pair. Hence, there is a finite probability that any given A_{1A} or A_{1B} site will be in the reduced state. Given midpoint potentials for the electron acceptors of −844 mV for A_{1B}, −671 mV for A_{1A}, −700 mV for F_X, −520 mV for F_A, and −580 mV for F_B (see ref 33), the application of the partition function states that the probability is 2.8×10^{-3} that the electron will reside on A_{1A} and 3.7×10^{-6} that the electron will reside on A_{1B} during this final state. In the absence of external donors and acceptors, the electron would be permanently distributed in this manner were it not for the existence of the recombination channel, which occurs to P_{700}^+ via a tunneling mechanism from A_{1A}^- or A_{1B}^-.[58] The electron will ultimately be bled from the acceptor chain and the PS I cofactors returned to the ground state.

The attachment of the $NQ(CH_2)_{15}S$−Pt adduct provides a third option for the electron on A_{1A}^- and A_{1B}^- (Figure 8). The

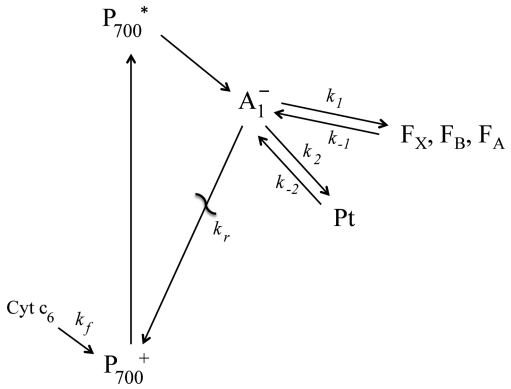

Figure 8. Energy diagram of the PS I−$NQ(CH_2)_{15}S$−Pt construct. The forward transfer of an electron to the iron−sulfur clusters is simplified as a single rate constant, k_1. See the text for details.

ability of the electron to be transferred through the molecular wire to the Pt nanoparticle will be a function of the forward rate constant, k_2, relative to the forward transfer of an electron to the iron−sulfur clusters (simplified here as a single rate constant, k_1) and the charge recombination channel, k_r. The rate of transfer of an electron from the quinone to the Pt nanoparticle, k_2, is governed by the driving force of the reaction (ΔG), the reorganization energy (λ), and the electronic coupling ($|V|^2$). A rough estimate of the driving force can be obtained by taking the difference between the midpoint potential of the quinone−semiquinone couple and midpoint potential of the proton−dihydrogen couple. There are no experimentally determined values for the midpoint potentials of A_{1A} or A_{1B}; instead, the calculated midpoint potentials of −671 mV for A_{1A} and −844 mV for A_{1B} will be used because the 173 mV difference in midpoint potentials agrees reasonably well with the experimentally determined rates of fast to slow electron transfer steps attributed to A_{1A}^- to F_X and A_{1B}^- to F_X, respectively (see ref 33 for a review). The proton−dihydrogen couple has a standard biochemical midpoint potential ($E^{\circ\prime}$) of −430 mV. Thus, the change in Gibbs free energy (ΔG) from A_{1A}^- is −241 mV and A_{1B}^- is −414 mV, and reduction of protons to dihydrogen will be highly favorable on both branches.

The reorganization energy (λ) associated with reduction of the Pt nanoparticle is likely to be very small because of the large surface area over which the electron is distributed. The effect on λ of changing the size of an electron acceptor has been studied by comparing fullerene (C_{60}) to smaller acceptors such as naphthalenediimide in donor−acceptor complexes.[59] As one might expect, C_{60} has a small reorganization energy because of the delocalization of the charge, and the same should apply for a Pt nanoparticle. Thus, the activation energy is expected to be relatively large. The electronic coupling is determined to a large extent by the distance between the naphthoquinone headgroup and the Pt nanoparticle. It is difficult to estimate this distance because of the number of variables involved, including the uncertain conformations of the methylene groups in the hydrocarbon chain. Ideally, the average distance between the center of the first and last carbon atoms of a freely rotating hydrocarbon would be $1.50l$, where l is the carbon−carbon distance of 1.54 Å.[60] The distance between the naphthoquinone headgroup and the Pt nanoparticle could therefore be as much as 22.5 Å were the hydrocarbon chain were to be fully extended. In contrast, the edge-to-edge distance between the quinones in the A_{1A} and A_{1B} sites is 9 Å. Given that the electronic coupling decreases exponentially with distance and a significant activation energy is expected, it is clear that under nearly all reasonable configurations of the molecular wire−Pt nanoparticle adduct, k_2 will be much smaller than k_1; hence, the electron will have only a small probability of being transferred to the Pt nanoparticle during forward electron transfer. This assessment is supported by the time-resolved optical data shown in Figure 4.

However, we also need to consider k_2, k_{-2}, and k_r. The relative magnitude of k_2 and k_r can be estimated from the kinetics of electron transfer in PS I in the absence of the iron−sulfur clusters. In PS I complexes from the *rubA* variant, which lacks F_X, F_A, and F_B but contains phylloquinone in the A_{1A} and A_{1B} sites, two kinetic phases are present with lifetimes of 15 and 95 μs.[61,62] The lifetimes of the $P_{700}^+A_{1A}^-$ and $P_{700}^+A_{1B}^-$ charge-separated states in the absence of F_X, F_A, and F_B are therefore 3 orders of magnitude shorter than the lifetime of the $P_{700}^+[F_A/F_B]^-$ charge-separated state in WT PS I. Although bidirectional electron transfer through the two branches of cofactors was not appreciated at the time of the *rubA* study, it seems reasonable that one kinetic phase is derived from $P_{700}^+A_{1A}^-$ recombination and the other from $P_{700}^+A_{1B}^-$ recombination. Given that the Gibbs free energy change between P_{700}^+ and A_{1B}^- is larger than that between P_{700}^+ and A_{1A}^-, and provided the reaction is in the normal region of the Marcus curve, we tentatively assign the 15 μs kinetic phase to the former while the 95 μs kinetic phase can be assigned to the latter. In the absence of F_X, F_A, and F_B, the electron on either A_{1A} or A_{1B} has only two available routes. It can either recombine with P_{700}^+ with rate constant k_r or be transferred to the Pt nanoparticle with rate constant k_2. The fate of the electron will be determined by the relative values of k_2 and k_r. While the value of k_2 is not known, the large distance between the naphthoquinone headgroup and the Pt nanoparticle as well as the presence of σ-bonds throughout the hydrocarbon tether will most certainly render k_2 much lower than k_r. This assessment is also supported by the time-resolved optical data shown in Figure 4.

We also need to consider the relative values of k_2 and k_{-2}. The k_2/k_{-2} ratio is given by the equation $k_2/k_{-2} = \exp(-\Delta G/kT)$; using our estimate for ΔG of −241 mV for the A branch and −414 mV for the B branch, we obtain a k_2/k_{-2} ratio of 10^4

dx.doi.org/10.1021/bi500104r | *Biochemistry* 2014, 53, 2295−2306

(A branch) or 10^7 (B branch). In either case, it is clear that this ratio is very large, and hence, the reverse transfer of an electron from the Pt nanoparticle to A_{1A} and/or A_{1B} is expected to be extremely slow and can be neglected. Because k_2 is much smaller than k_r and k_1, the transfer of an electron to the Pt nanoparticle can occur only if charge recombination is inhibited. The reduction of P_{700}^+ by cytochrome c_6, which occurs on the millisecond time scale, is faster than charge recombination from $[F_A/F_B]^-$, which occurs with a lifetime of 65 ms. Thus, the recombination channel, k_r, can be eliminated when the iron−sulfur clusters are present. Under these conditions, the lifetime of the electron on the acceptor chain becomes very long, and we propose that a small leak through the span of the molecular wire allows electrons to be transferred to the Pt nanoparticle.[10] Because k_{-2} is negligible, the electrons become trapped. The rate of trapping is given by $k_{-1}(k_2/k_1)$. These rate constants are not known accurately, but k_1 is on the order of 10^7 s^{-1}. In the absence of the iron−sulfur clusters, the charge recombination from A_{1A}^- occurs with a lifetime of 95 μs, so $k_r \approx 10^4$ s^{-1}. Using these two values, the observed lifetime of 65 ms for the back reaction from F_B in native PS I yields a k_{-1} of $\approx 1.6 \times 10^4$ s^{-1}. If we arbitrarily assume that k_2 is 1 order of magnitude smaller than k_r, we obtain a rate of ~ 1 s^{-1} for the trapping of electrons on the Pt nanoparticle. When two electrons are serially transferred to the Pt nanoparticle, the release of dihydrogen makes electron transfer irreversible, thereby depleting the acceptor side of electron(s) until the next photon strikes the reaction center.

This work adds to the number of practical methods for attaching a Pt nanoparticle to the acceptor side of PS I for the purpose of achieving light-driven hydrogen evolution. These include self-organized platinization, the electrostatic attachment of a Pt nanoparticle, the attachment of a Pt nanoparticle via a molecular wire to the F_B cluster, and, now, the attachment of a Pt nanoparticle via a molecular wire to the A_{1A} and A_{1B} binding sites. Although the selection of which method to choose for a particular device will depend on the details of the application, the wide variety of attachment points demonstrates the versatility of PS I as a photocatalyst for solar hydrogen production.

■ ASSOCIATED CONTENT

Supporting Information

Chemical synthesis and characterization of 1-[15-(3-methyl-1,4-naphtoquinone-2-yl)]pentadecyl disulfide. This material is available free of charge via the Internet at http://pubs.acs.org.

■ AUTHOR INFORMATION

Corresponding Authors

*E-mail: jhg5@psu.edu. Phone: (814) 865-1163.
*E-mail: avde@brocku.ca. Phone: (905) 688-5550.

Author Contributions

M.G. and J.S. contributed equally to this work.

Funding

Support for the construction and evaluation of the PS I−$NQ(CH_2)_{15}S$−Pt nanoconstruct was provided by the U.S. Air Force Office of Scientific Research (AFOSR) via Grant FA9550-09-1-0671 (J.H.G.), and support for the cytochrome donation study was provided by the U.S. Department of Energy, Basic Energy Sciences, Division of Materials Sciences and Engineering, under Contract DE-FG02-05ER46222 (J.H.G.). Support by the German Federal Ministry of Education and Research (BMBF, Project "H_2 design cells") and the EU/NEST project "Solar-H2" (M.R.) and by the Natural Sciences and Engineering Research Council of Canada in the form of a Discovery Grant (A.v.d.E.) is gratefully acknowledged.

Notes

The authors declare no competing financial interest.

■ ACKNOWLEDGMENTS

We thank Dr. Junlei Sun for assistance in conducting the time-resolved optical measurements at 480 nm and Dr. Carolyn Lubner and Prof. Ron Koder for valuable discussions.

■ REFERENCES

(1) Heathcote, P., Jones, M. R., and Fyfe, P. K. (2003) Type I photosynthetic reaction centres: Structure and function. *Philos. Trans. R. Soc., B 358*, 231−243.

(2) Golbeck, J. (2006) *Photosystem I: The Light-Driven Plastocyanin:Ferredoxin Oxidoreductase*, Springer, Dordrecht, The Netherlands.

(3) Sun, A. S. K., and Sauer, K. (1971) Pigment systems and electron transport in chloroplasts. 1. Quantum requirements for 2 light reactions in spinach chloroplasts. *Biochim. Biophys. Acta 234*, 399−405.

(4) Brettel, K. (1997) Electron transfer and arrangement of the redox cofactors in photosystem I. *Biochim. Biophys. Acta 1318*, 322−373.

(5) Greenbaum, E. (1985) Platinized chloroplasts: A novel photocatalytic material. *Science 230*, 1373−1375.

(6) Greenbaum, E. (1988) Interfacial photoreactions at the photosnthetic membrane interface: An upper limit for the number of platinum atoms required to form a hydrogen-evolving platinum metal complex. *J. Phys. Chem. 92*, 4571−4574.

(7) Lee, J. W., Tevault, C. V., Blankinship, S. L., Collins, R. T., and Greenbaum, E. (1994) Photosynthetic watersplitting: In situ photoprecipitation of metallocatalysts for photoevolution of hydrogen and oxygen. *Energy Fuels 8*, 770−773.

(8) Millsaps, J. F., Bruce, B. D., Lee, J. W., and Greenbaum, E. (2001) Nanoscale photosynthesis: Photocatalytic production of hydrogen by platinized photosystem I reaction centers. *Photochem. Photobiol. 73*, 630−635.

(9) Evans, B. R., O'Neill, H. M., Hutchens, S. A., Bruce, B. D., and Greenbaum, E. (2004) Enhanced photocatalytic hydrogen evolution by covalent attachment of plastocyanin to photosystem I. *Nano Lett. 4*, 1815−1819.

(10) Lee, J. W., Lee, I., and Greenbaum, E. (2005) Imaging nanometere metallocatalysts fromed by photosynthetic deposition of water-soluble transition-metal compounds. *J. Phys. Chem. B 109*, 5409−5413.

(11) Iwuchukwu, I. J., Vaughn, M., Myers, N., O'Neill, H., Frymier, P., and Bruce, B. D. (2010) Self-organized photosynthetic nanoparticle for cell-free hydrogen production. *Nat. Nanotechnol. 5*, 73−79.

(12) Yehezkeli, O., Wilner, O. I., Tel-Vered, R., Roizman-Sade, D., Nechushtai, R., and Willner, I. (2010) Generation of photocurrents by bis-aniline-cross-linked Pt nanoparticle/photosystem I composites on electrodes. *J. Phys. Chem. B 114*, 14383−14388.

(13) Utschig, L. M., Dimitrijevic, N. M., Poluektov, O. G., Chemerisov, S. D., Mulfort, K. L., and Tiede, D. M. (2011) Photocatalytic hydrogen production from noncovalent biohybrid Photosystem I/Pt nanoparticle complexes. *J. Phys. Chem. Lett. 2*, 236−241.

(14) LeBlanc, G., Chen, G., Jennings, G. K., and Cliffel, D. E. (2012) Photoreduction of catalytic platinum particles using immobilized multilayers of Photosystem I. *Langmuir 28*, 7952−7956.

(15) Efrati, A., Yehezkeli, O., Tel-Vered, R., Michaeli, D., Nechushtai, R., and Willner, I. (2012) Electrochemical switching of photoelectrochemical processes at CdS QDs and photosystem I-modified electrodes. *ACS Nano 6*, 9258−9266.

(16) Ihara, M., Nakamoto, H., Kamachi, T., Okura, I., and Maeda, M. (2006) Photoinduced hydrogen production by direct electron transfer

from photosystem I cross-linked with cytochrome c_3 to [NiFe]-hydrogenase. *Photochem. Photobiol. 82*, 1677−1685.
(17) Ihara, M., Nishihara, H., Yoon, K. S., Lenz, O., Friedrich, B., Nakamoto, H., Kojima, K., Honma, D., Kamachi, T., and Okura, I. (2006) Light-driven hydrogen production by a hybrid complex of a [NiFe]-hydrogenase and the cyanobacterial photosystem I. *Photochem. Photobiol. 82*, 676−682.
(18) Krassen, H., Schwarze, A., Friedrich, B., Ataka, K., Lenz, O., and Heberle, J. (2009) Photosynthetic hydrogen production by a hybrid complex of photosystem I and [NiFe]-hydrogenase. *ACS Nano 3*, 4055−4061.
(19) Grimme, R. A., Lubner, C. E., Bryant, D. A., and Golbeck, J. H. (2008) Photosystem I/molecular wire/metal nanoparticle bioconjugates for the photocatalytic production of H_2. *J. Am. Chem. Soc. 130*, 6308−6309.
(20) Grimme, R. A., Lubner, C. E., and Golbeck, J. H. (2009) Maximizing H_2 production in Photosystem I/dithiol molecular wire/platinum nanoparticle bioconjugates. *Dalton Trans. 45*, 10106−10113.
(21) Lubner, C. E., Grimme, R., Bryant, D. A., and Golbeck, J. H. (2010) Wiring photosystem I for direct solar hydrogen production. *Biochemistry 49*, 404−414.
(22) Lubner, C. E., Knorzer, P., Silva, P. J., Vincent, K. A., Happe, T., Bryant, D. A., and Golbeck, J. H. (2010) Wiring an [FeFe]-hydrogenase with Photosystem I for light-induced hydrogen production. *Biochemistry 49*, 10264−10266.
(23) Lubner, C. E., Applegate, A. M., Knorzer, P., Ganago, A., Bryant, D. A., Happe, T., and Golbeck, J. H. (2011) Solar hydrogen-producing bionanodevice outperforms natural photosynthesis. *Proc. Natl. Acad. Sci. U.S.A. 108*, 20988−20991.
(24) Lubner, C., Bryant, D. A., and Golbeck, J. H. (2011) Wired reaction centers. In *Molecular Solar Fuels* (Hillier, W., and Wydrzynski, T., Eds.) pp 464−505, Royal Society of Chemistry, London.
(25) Ikegami, I., and Katoh, S. (1975) Enrichment of photosystem I reaction center chlorophyll from spinach chloroplasts. *Biochim. Biophys. Acta 376*, 588−592.
(26) Itoh, S., Iwaki, M., and Ikegami, I. (1987) Extraction of vitamin K_1 from photosystem I particles by treatment with diethyl ether and its effects on the A_1^- EPR signal and system I photochemistry. *Biochim. Biophys. Acta 893*, 508−516.
(27) Ikegami, I., and Katoh, S. (1989) Preparation and characterization of P700-enriched photosystem-I complexes from the thermophilic cyanobacterium, *Synechococcus* sp. *Plant Cell Physiol. 30*, 175−182.
(28) Ikegami, I., Itoh, S., and Iwaki, M. (1995) Photoactive photosystem I particles with a molar ratio of chlorophyll α to P700 of 9. *Plant Cell Physiol. 36*, 857−864.
(29) Ikegami, I., Itoh, S., and Iwaki, M. (2000) Selective extraction of antenna chlorophylls, carotenoids and quinones from photosystem I reaction center. *Plant Cell Physiol. 41*, 1085−1095.
(30) Itoh, S., Iwaki, M., and Ikegami, I. (2001) Modification of Photosystem I reaction center by the extraction and exchange of chlorophylls and quinones. *Biochim. Biophys. Acta 1507*, 115−138.
(31) Biggins, J., and Mathis, P. (1988) Functional role of vitamin K_1 in photosystem I of the cyanobacterium *Synechocystis* 6803. *Biochemistry 27*, 1494−1500.
(32) Biggins, J. (1990) Evaluation of selected benzoquinones, naphthoquinones, and anthraquinones as replacements for phylloquinone in the A_1 acceptor site of the photosystem I reaction center. *Biochemistry 29*, 7259−7264.
(33) Srinivasan, N., and Golbeck, J. H. (2009) Protein-cofactor interactions in bioenergetic complexes: The role of the A_{1A} and A_{1B} phylloquinones in Photosystem I. *Biochim. Biophys. Acta 1787*, 1057−1088.
(34) Kim, D., Yoshihara, K., and Ikegami, I. (1989) Picosecond photochemistry of P700-enriched and vitamin K_1-depleted photosystem I particles isolated from spinach. *Plant Cell Physiol. 30*, 679−684.
(35) Itoh, S., and Iwaki, M. (1988) Delayed fluorescence in photosystem I enhanced by phylloquinone (vitamin K-1) extraction with ether. *Biochim. Biophys. Acta 934*, 32−38.
(36) Iwaki, M., and Itoh, S. (1989) Electron transfer in spinach photosystem I reaction center containing benzo-, naphtho- and anthraquinones in place of phylloquinone. *FEBS Lett. 256*, 11−16.
(37) Rustandi, R., Snyder, S., Biggins, J., Norris, J., and Thurnauer, M. (1992) Reconstitution and exchange of quinones in the A_1 Site of Photosystem-I: An electron spin polarization electron paramagnetic resonance study. *Biochim. Biophys. Acta 1101*, 311−320.
(38) Sieckman, I., Van der Est, A., Bottin, H., Setif, P., and Stehlik, D. (1991) Nanosecond electron transfer kinetics in photosystem I following substitution of quinones for vitamin K_1 as studied by time resolved EPR. *FEBS Lett. 284*, 98−102.
(39) Terasaki, N., Yamamoto, N., Tamada, K., Hattori, M., Hiraga, T., Tohri, A., Sato, I., Iwai, M., Iwai, M., Taguchi, S., Enami, I., Inoue, Y., Yamanoi, Y., Yonezawa, T., Mizuno, K., Murata, M., Nishihara, H., Yoneyama, S., Minakata, M., Ohmori, T., Sakai, M., and Fujii, M. (2007) Bio-photosensor: Cyanobacterial photosystem I coupled with transistor via molecular wire. *Biochim. Biophys. Acta 1767*, 653−659.
(40) Johnson, T. W., Shen, G., Zybailov, B., Kolling, D., Reategui, R., Beauparlant, S., Vassiliev, I. R., Bryant, D. A., Jones, A. D., Golbeck, J. H., and Chitnis, P. R. (2000) Recruitment of a foreign quinone into the A_1 site of Photosystem I. I. Genetic and physiological characterization of phylloquinone biosynthetic pathway mutants in *Synechocystis* sp. PCC 6803. *J. Biol. Chem. 275*, 8523−8530.
(41) Semenov, A. Y., Vassiliev, I. R., van der Est, A., Mamedov, M. D., Zybailov, B., Shen, G., Stehlik, D., Diner, B. A., Chitnis, P. R., and Golbeck, J. H. (2000) Recruitment of a foreign quinone into the A_1 site of Photosystem I. Altered kinetics of electron transfer in phylloquinone biosynthetic pathway mutants studied by time-resolved optical, EPR, and electrometric techniques. *J. Biol. Chem. 275*, 23429−23438.
(42) Zybailov, B., van der Est, A., Zech, S. G., Teutloff, C., Johnson, T. W., Shen, G., Bittl, R., Stehlik, D., Chitnis, P. R., and Golbeck, J. H. (2000) Recruitment of a foreign quinone into the A_1 site of Photosystem I. II. Structural and functional characterization of phylloquinone biosynthetic pathway mutants by electron paramagnetic resonance and electron-nuclear double resonance spectroscopy. *J. Biol. Chem. 275*, 8531−8539.
(43) Johnson, T. W., Zybailov, B., Jones, A. D., Bittl, R., Zech, S., Stehlik, D., Golbeck, J. H., and Chitnis, P. (2001) Recruitment of a foreign quinone into the A_1 site of Photosystem I. *In vivo* replacement of plastoquinone-9 by media-supplemented naphthoquinones in phylloquinone biosynthetic pathway mutants of *Synechocystis* sp. PCC 6803. *J. Biol. Chem. 276*, 31512−31521.
(44) Johnson, W. T., Naithani, S., Stewart, C., Zybailov, B., Daniel Jones, A., Golbeck, J. H., and Chitnis, P. R. (2003) The *menD* and *menE* homologs code for 2-succinyl-6-hydroxyl-2,4-cyclohexadiene-1-carboxylate synthase and O-succinylbenzoic acid-CoA synthase in the phylloquinone biosynthetic pathway of *Synechocystis* sp. PCC 6803. *Biochim. Biophys. Acta 1557*, 67−76.
(45) Pushkar, Y. N., Golbeck, J. H., Stehlik, D., and Zimmermann, H. (2004) Asymmetric hydrogen-bonding of the quinone cofactor in photosystem I probed by C-13-labeled naphthoquinones. *J. Phys. Chem. B 108*, 9439−9448.
(46) Karyagina, I., Golbeck, J. H., Srinivasan, N., Stehlik, D., and Zimmermann, H. (2006) Single-sided hydrogen bonding to the quinone cofactor in photosystem I probed by selective C-13-labelled naphthoquinones and transient EPR. *Appl. Magn. Reson. 30*, 287−310.
(47) Sakuragi, Y., Zybailov, B., Shen, G., Bryant, D. A., Golbeck, J. H., Diner, B. A., Karygina, I., Pushkar, Y., and Stehlik, D. (2005) Recruitment of a foreign quinone into the A_1 site of photosystem I. Characterization of a *menB rubA* double deletion mutant in *Synechococcus* sp. PCC 7002 devoid of F_X, F_A, and F_B and containing plastoquinone or exchanged 9,10-anthraquinone. *J. Biol. Chem. 280*, 12371−12381.

(48) Chen, S. H., and Kimura, K. (2001) Synthesis of thiolate-stabilized platinum nanoparticles in protolytic solvents as isolable colloids. *J. Phys. Chem. B 105*, 5397−5403.
(49) Rögner, M., Nixon, P. J., and Diner, B. A. (1990) Purification and characterization of photosystem I and photosystem II core complexes from wild-type and phycocyanin-deficient strains of the cyanobacterium *Synechocystis* PCC 6803. *J. Biol. Chem. 265*, 6189−6196.
(50) Vassiliev, I. R., Jung, Y. S., Mamedov, M. D., Semenov, A., and Golbeck, J. H. (1997) Near-IR absorbance changes and electrogenic reactions in the microsecond-to-second time domain in Photosystem I. *Biophys. J. 72*, 301−315.
(51) van der Est, A. (2009) Transient EPR: Using spin polarization in sequential radical pairs to study electron transfer in photosynthesis. *Photosynth. Res. 102*, 335−347.
(52) Niklas, J., Epel, B., Antonkine, M. L., Sinnecker, S., Pandelia, M. E., and Lubitz, W. (2009) Electronic structure of the quinone radical anion $A_1^{\bullet-}$ of Photosystem I investigated by advanced pulse EPR and ENDOR techniques. *J. Phys. Chem. B 113*, 10367−10379.
(53) Xu, W., Chitnis, P., Valieva, A., van der Est, A., Pushkar, Y. N., Krzystyniak, M., Teutloff, C., Zech, S. G., Bittl, R., Stehlik, D., Zybailov, B., Shen, G., and Golbeck, J. H. (2003) Electron transfer in cyanobacterial Photosystem I: I. Physiological and spectroscopic characterization of site-directed mutants in a putative electron transfer pathway from A_0 through A_1 to F_X. *J. Biol. Chem. 278*, 27864−27875.
(54) Shinkarev, V. P., Zybailov, B., Vassiliev, I. R., and Golbeck, J. H. (2002) Modeling of the $P700^+$ charge recombination kinetics with phylloquinone and plastoquinone-9 in the A_1 site of Photosystem I. *Biophys. J. 83*, 2885−2897.
(55) Rappaport, F., Diner, B. A., and Redding, K. (2006) Optical Measurements of Secondary Electron Transfer in Photosystem I. In *Photosystem I: The Light-Induced Plastocyanin:Ferredoxin Oxidoreductase* (Golbeck, J., Ed.) pp 223−244, Springer, Dordrecht, The Netherlands.
(56) Bautista, J. A., Rappaport, F., Guergova-Kuras, M., Cohen, R. O., Golbeck, J. H., Wang, J. Y., Beal, D., and Diner, B. A. (2005) Biochemical and biophysical characterization of Photosystem I from phytoene desaturase and ζ-carotene desaturase deletion mutants of *Synechocystis* sp. PCC 6803: Evidence for PsaA- and PsaB-side electron transport in cyanobacteria. *J. Biol. Chem. 280*, 20030−20041.
(57) Redding, K., and van der Est, A. (2006) The directionality of electron transport in Photosystem I. In *Photosystem I: The Light-Induced Plastocyanin:Ferredoxin Oxidoreductase* (Golbeck, J., Ed.) pp 413−437, Springer, Dordrecht, The Netherlands.
(58) Shinkarev, V. P. (2006) Functional modeling of electron transfer in photosynthetic reaction centers. In *Photosystem I: The Light-Driven Plastocyanin:Ferredoxin Oxidoreductase* (Golbeck, J. H., Ed.) pp 611−637, Springer, Dordrecht, The Netherlands.
(59) Imahori, H. (2004) Porphyrin-fullerene linked systems as artificial photosynthetic mimics. *Org. Biomol. Chem. 2*, 1425−1433.
(60) Laskowski, L., and Burk, R. E. (1939) The probable length of hydrocarbon chains. *J. Chem. Phys. 7*, 465−469.
(61) Shen, G., Antonkine, M. L., van der Est, A., Vassiliev, I. R., Brettel, K., Bittl, R., Zech, S. G., Zhao, J., Stehlik, D., Bryant, D. A., and Golbeck, J. H. (2002) Assembly of Photosystem I. II. Rubredoxin is required for the *in vivo* assembly of F_X in *Synechococcus* sp. PCC 7002 as shown by optical and EPR spectroscopy. *J. Biol. Chem. 277*, 20355−20366.
(62) Shen, G., Zhao, J., Reimer, S. K., Antonkine, M. L., Cai, Q., Weiland, S. M., Golbeck, J. H., and Bryant, D. A. (2002) Assembly of Photosystem I. I. Inactivation of the *rubA* gene encoding a membrane-associated rubredoxin in the cyanobacterium *Synechococcus* sp. PCC 7002 causes a loss of Photosystem I activity. *J. Biol. Chem. 277*, 20343−20354.